

RESEARCH ARTICLE

Ultra-wideband fluidically steered antipodal Vivaldi antenna array

Ian Goode  | Carlos E. Saavedra

Department of Electrical and Computer Engineering, Queen's University, Ontario, Canada

Correspondence

Ian Goode, Department of Electrical and Computer Engineering, Queen's University, Kingston, Ontario K7L 3N6, Canada.

Email: ian.goode@queensu.ca

Funding information

Natural Sciences and Engineering Research Council of Canada, Grant/Award Number: #RGPIN-2016-04784

Abstract

An ultra-wideband 1×4 antipodal Vivaldi antenna array with microfluidic beam steering is reported. The antipodal configuration is selected for its microstrip feed line, which is convenient for implementation of the phase-shifting structure. Each antenna element uses a true-time-delay phase shifter consisting of nine microfluidic channels under its feed line in which deionized (DI) water, $\epsilon_r = 77 + j13$ ($\tan\delta = 0.17$) at 3 GHz, is pumped to change the speed of the propagating wave. The array was fabricated using a 1.52 mm thick substrate with $\epsilon_r = 3.55$ and $\tan\delta = 0.0027$. Each antenna element and phase shifter measures 55 mm \times 140 mm. Measurements show that the array yields up to 90° of beam steering from 3 to 6.5 GHz and up to 40° of steering from 6.5 to 10 GHz. The array has a maximum realized gain of 13.1 dBi, and a half-power beamwidth of less than 40° for all configurations.

KEYWORDS

beam steering, dielectric fluid, microwave microfluidics, phased antenna array, Vivaldi antenna

1 | INTRODUCTION

Phased antenna arrays are often found in systems that handle moderate to high amounts of RF power such as radars.

The use of fluidic techniques to implement beam steering in antenna arrays is a compelling subject of investigation because fluids do not degrade the power-handling capability of the system nor do they introduce any appreciable amount of distortion relative to semiconductor devices. Only a few studies have been published using isotropic homogeneous fluidic beam-steering methods.^{1–4} In Reference 1, a patch antenna is located in a solid cavity with a partially reflecting top wall. Water is pumped into channels inside the cavity to change the direction of the radiated beam. The structure in Reference 2 uses a planar Yagi-Uda antenna with a movable liquid metal reflector to steer the beam. In Reference 3, a four-element scanning patch array is described but only simulation results are reported. A patch antenna loaded with metal slugs that are moved inside a fluidic channel is proposed in Reference 4. The operating bandwidth in these previous studies is below 0.1 GHz and the maximum antenna gain is below 5.7 dBi.

This paper reports the first known fluidic beam-steering array employing Vivaldi antennas and delivering a measured operating bandwidth of 7 GHz, covering the 3 to 10 GHz band. The array exhibits a measured beam-steering range of up to 90° from 3 to 6.5 GHz and up to 40° of steering from 6.5 to 10 GHz along the \vec{H} -plane. The maximum realized gain across the full 3 to 10 GHz band is 13.1 dBi when no channels are filled with water and the beam is pointing at boresight. The minimum realized peak gain of the array is 7 dBi when the beam is at $\pm 45^\circ$ and the maximum number of channels are filled with water.

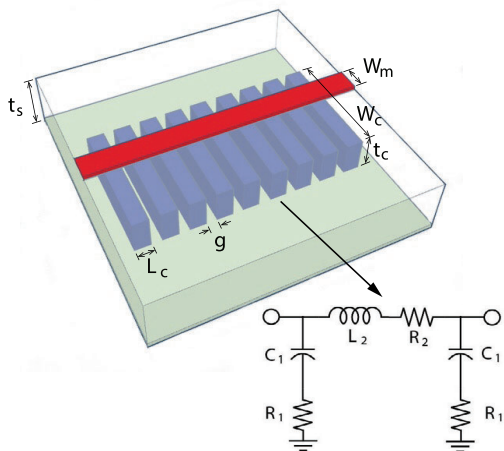
2 | FLUIDICALLY-STEERED ARRAY DESIGN

The fluidic true-time delay phase shifter used here is depicted in Figure 1.^{5,6} It consists of a set of nine channels under a microstrip transmission line that are filled with fluid. The structure has a total length of $9L_c + 8g = 45.6$ mm. The transmission line width is 3.4 mm which corresponds to a 50 Ω impedance on a 1.52-mm thick substrate with $\epsilon_r = 3.55$ (Rogers 4003C). In practice, the channels were milled through the ground plane of the substrate during fabrication (Section 3) and the ground plane lost during milling was restored using copper tape to maintain electrical continuity and to seal the water in the channels. Therefore, the spacing, g , between the channels of the fluidic phase shifter was chosen to provide enough bonding area for the copper tape without making the phase shifting section excessively

long. Through testing, a g value of 1.2 mm resulted in a satisfactory fluidic seal between channels, and sufficient bonding area to repair the ground plane. The height and width of the channels t_c and W_c were chosen in simulation to provide ample phase shift without the loaded channels giving a large impedance mismatch. It was found that having shorter channels (small t_c) resulted in a smaller discontinuity in impedance when the channels were air or water loaded, but the channels needed to be tall enough to produce an ample phase shift. The channel widths were chosen to provide enough total phase shift and sufficient resolution in the phase shift per channel.

DI water was chosen as the dielectric fluid in this work because its high permittivity of $\epsilon_r = 77 + j13^7$ (which is plotted over frequency in Figure 2) yields a significant time delay on the propagating wave with only small amounts of fluid. The phase-shifter's simulated response using ANSYS HFSS from 3 to 10 GHz is shown in Figure 3. As expected, the insertion loss increases with frequency as more channels are filled with water due the rise of its loss tangent, which ultimately impacts the gain of the antenna and the useful beam-steering range of the array at higher frequencies. Therefore, while all nine water channels were used between 3 and 6.5 GHz, at most only six channels were filled with water between 6.5 and 8 GHz and at most three channels were filled between 8 and 10 GHz to keep the phase-shifter loss within an acceptable level. Thus, only the black data trends in Figure 3 were used in the array. The phase shifting response of the fluidic structure is plotted relative to the air-filled case and is shown in Figure 3B.

$$y_1(t) = 0.4e^{0.21t} - 1.3 \quad (1)$$



var.	L_c	W_c	t_c	g	W_m	t_s	ϵ_r
(mm)	4.0	30	1.0	1.2	3.4	1.52	3.55

FIGURE 1 Schematic of the nine-channel fluidic true-time delay phase-shifter. Each fluidic channel can be modeled using the lumped-element equivalent circuit shown following the procedure in Reference 5 [Color figure can be viewed at wileyonlinelibrary.com]

$$z_1(t) = 3.6t + 75 \quad (2)$$

$$y_2(t) = 0.4e^{0.23t} - 1.3 \quad (3)$$

$$z_2(t) = 1.9t + 75 \quad (4)$$

$$y_3(t) = 0.1e^{-(t-18)/3.2} + 1.6 \quad (5)$$

$$z_3(t) = t + 57 \quad (6)$$

$$t = 0 : 18 \quad (7)$$

An antipodal Vivaldi element was chosen for this investigation because its microstrip transmission-line feed is convenient for fluidic phase shifting. Figure 4 shows the design of a single element with the phase shifting section from Figure 1. The dimensions and the parametric equations in (1)–(7) are used to express the contours of the Vivaldi element in mm.

For the antenna array, the first design choice was to select whether to arrange the antennas along their \vec{H} -planes or \vec{E} -planes. The \vec{H} -plane corresponds to the x -axis and the \vec{E} -plane to the y -axis in Figure 5. An \vec{E} -plane alignment would yield a narrower beamwidth along that plane and provide easier access to the fluidic channels for watering and de-watering. Nonetheless, due to the width of the elements used here, they would be located more than $\lambda/2$ apart from each other at the upper-end of the frequency band, thereby introducing unacceptably large grating lobes. Therefore, the elements were lined-up along their \vec{H} -planes and were located 15 mm apart from each other. This distance was chosen, as it is half a free space wavelength at 10 GHz. The 3D model of the four-element Vivaldi array configuration is depicted in Figure 5. Aligning the elements in the \vec{H} -plane the narrows the beam compared to the single element. Also, since the single element is less directional in the \vec{H} -plane, this allows for a more uniform gain response with beam steering.

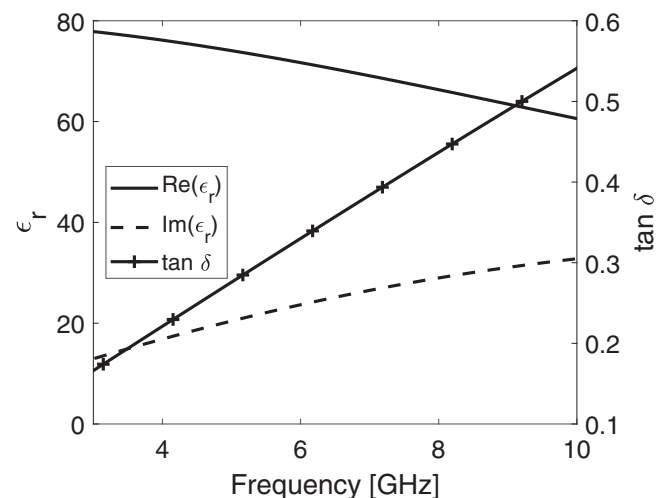


FIGURE 2 Model of relative permittivity of deionized water at 20°C⁷

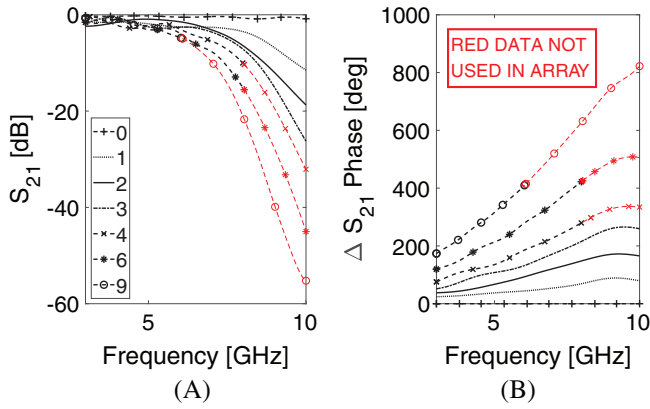


FIGURE 3 A, Simulated insertion loss with legend showing the number of channels that are water-filled corresponding to all cases used in Figure 6 and B, simulated phase response. Simulations carried out using the water model from Reference 7. The data in red shows that bandwidth over which certain filling combinations were not used [Color figure can be viewed at wileyonlinelibrary.com]

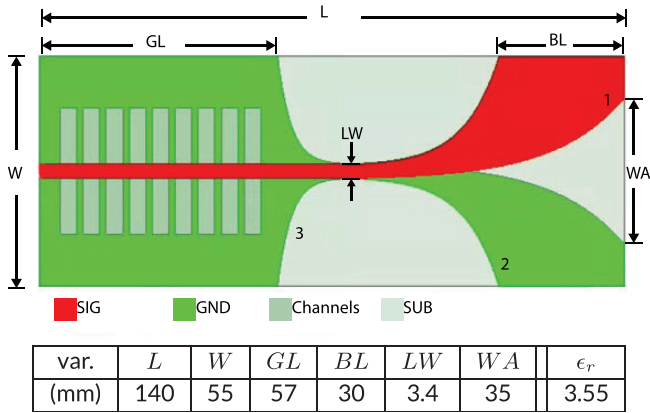


FIGURE 4 HFSS model of the single element, showing a top view with legend depicting layers with the same channel dimensions and spacing as Figure 1. The equations describing the shape of the contour curves 1 through 3 are given in Equations (1)-(7) [Color figure can be viewed at wileyonlinelibrary.com]

There are a wide number of channel-filling combinations available for beam steering with the proposed array. Here, a small subset of seven channel-filling arrangements was selected to demonstrate the beam-steering effect. A diagram of the filling arrangements for the four antenna elements is shown in Figure 6. The baseline arrangement, shown in the middle of the figure, is labeled “Air” and corresponds to the case where all channels in all four antennas are empty of water. For this case, the antenna beam points at boresight ($\theta = 0$). To steer the beam in the $+\theta$ direction, the 1R to 3R arrangements are used. For arrangement 1R, the number of filled channels is 0-1-2-3 for antenna elements $a_1 a_2 a_3 a_4$ where a_1 is used as the reference and the remaining elements have a uniform phase progression. For case 2R, the number of filled channels is 0-2-4-6 and for 3R, there are 0-3-6-9 filled channels with a_1 again used as the reference element.

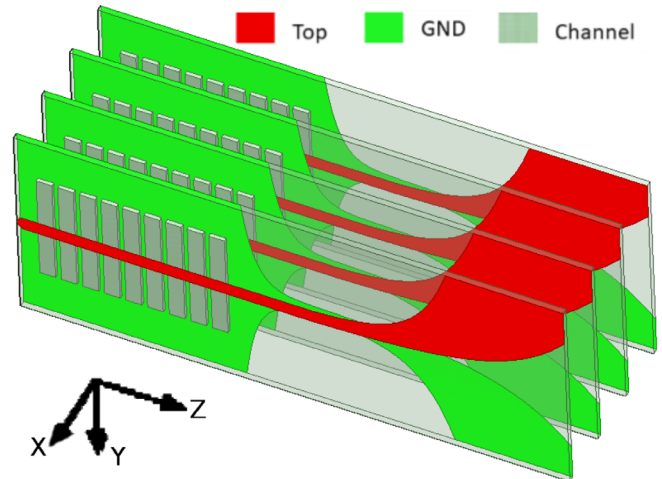


FIGURE 5 HFSS simulation model of the four-element array showing four elements and nine water channels per element, the four elements are each 15 mm apart [Color figure can be viewed at wileyonlinelibrary.com]

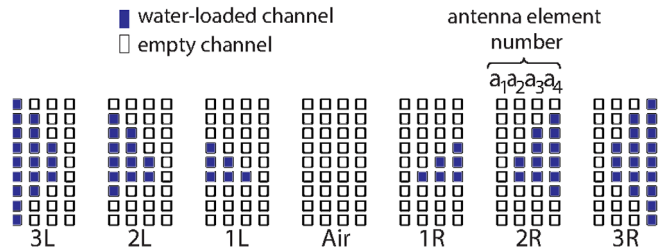


FIGURE 6 Diagram showing the channel filling under each filling state, where the labels below each case correspond to the legend in the beam-steering measurements and the bottom row of channels are closed to the RF port of the antenna [Color figure can be viewed at wileyonlinelibrary.com]

To steer the beam in the $-\theta$ direction, the filling arrangements 1L to 3L were used which are mirror images of the 1R-3R cases. Certainly, there are many other filling orders that can produce a uniform phase progression between the elements such as 0-0-1-1, 0-0-2-2, ... or their reverse 1-1-0-0, ... etc. Such arrangements can produce beam-steering angles that are in-between those produced by the filling sequences depicted in Figure 6.

3 | EXPERIMENTAL RESULTS

The antennas were fabricated in-house using a computer controlled milling machine from LPKF Laser & Electronics AG. Radiation pattern measurements were taken at Queen’s University’s anechoic chamber which reports realized gain. Antenna return loss measurements were taken using an Anritsu MS4644B vector network analyzer calibrated using an Anritsu 3652A-2 coaxial calibration kit.

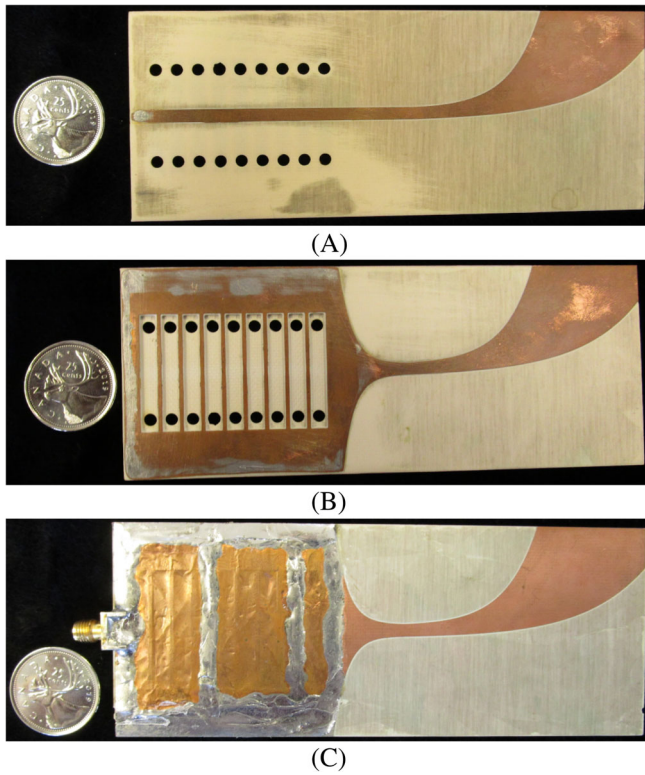


FIGURE 7 A, Top view of a single element, B, bottom view without RF connector and without copper tape to reveal the channels in the phase shifter section, C, bottom of element with RF connector and copper tape to show how the phase shifting channels were covered to repair the ground plane and seal the water into the channels [Color figure can be viewed at wileyonlinelibrary.com]

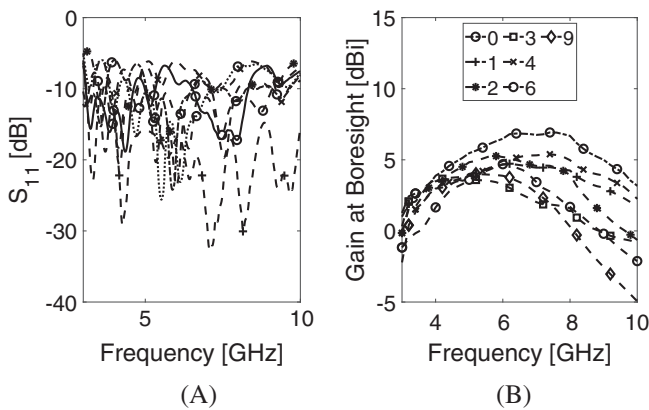


FIGURE 8 A, Measured return loss of the single element, B, measured maximum gain of the single element vs frequency, legend shows number of channels water filled, only the numbers of channels that were filled in Figure 6 are plotted

A photograph of a fabricated antenna element is depicted in Figure 7. Holes were drilled at both ends of the channels to add water and allow air to escape as water is added. To prevent water from draining from the channels when the antenna is vertically oriented, the holes were sealed with hot

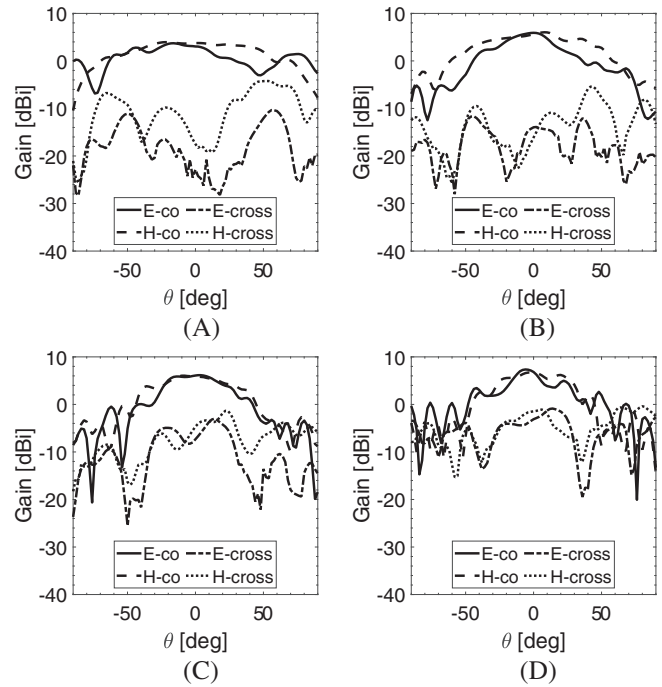


FIGURE 9 Measured radiation patterns at four different frequencies for the single base element depicted in Figure 5 with all channels air filled. A, 4 GHz B, 5 GHz C, 7 GHz and D, 9 GHz

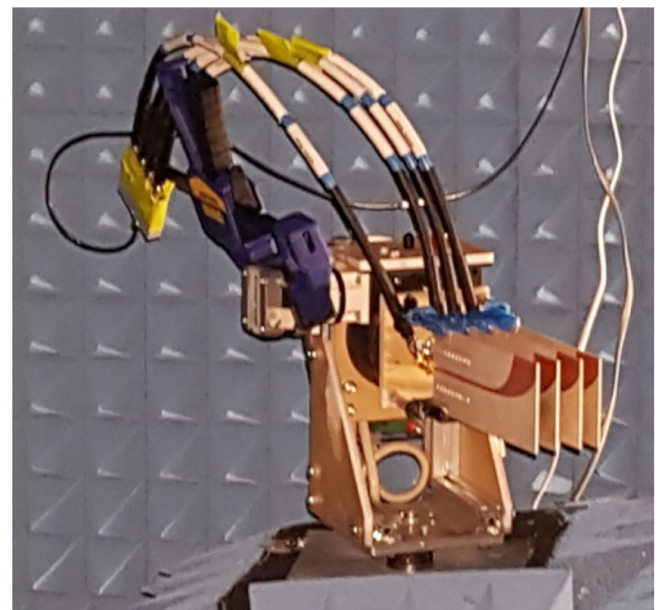


FIGURE 10 Four-element array in the anechoic chamber showing vertical or X-Z polarization in the all air-filled configuration [Color figure can be viewed at wileyonlinelibrary.com]

glue during testing. Being far away from the transmission line feed, the glue has a negligible impact on the response of the antenna. For this proof of concept each channel was filled or emptied of water manually using a syringe. The process could be automated using either micropumps or

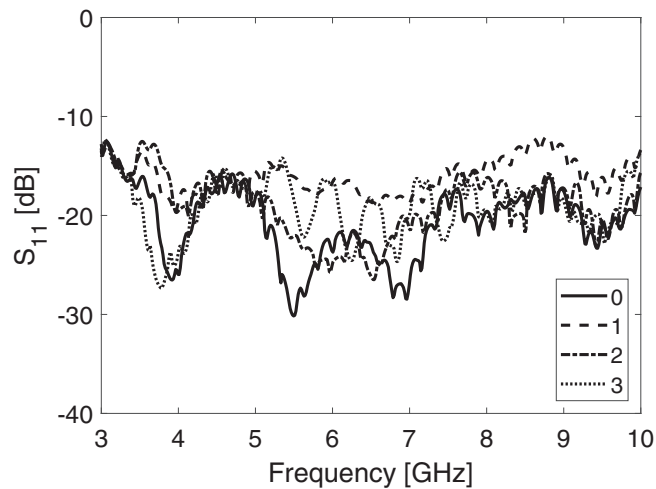


FIGURE 11 Measured array input reflection through the port of the power splitter, legend shows the number of channels of phase progression between each element

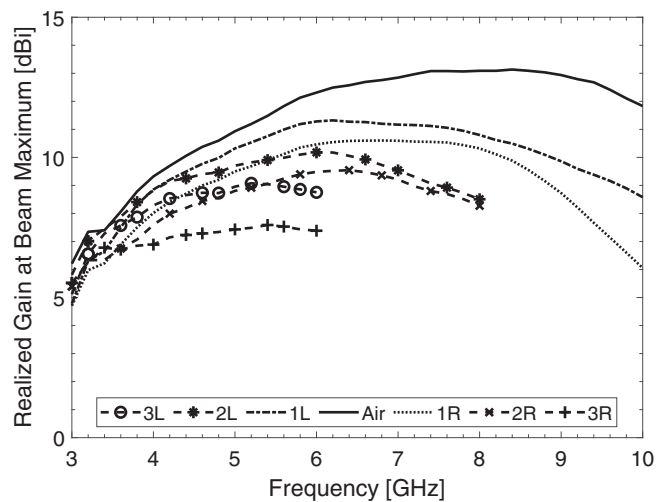


FIGURE 12 Measured realized gain at beam maximum the legend shows the same channel filling combinations as Figure 6

electrowetting techniques to route the water. Figure 8A shows the measured input reflection data for a single element under all used channel-filling combinations and Figure 8B shows the measured maximum gain for the single element. Only a subset of channels are filled, the gain decreases for the single element as more water is added due to its loss tangent. Four radiation patterns with cross-polarization measurements are seen in Figure 9, showing the performance of the single antenna element. Each of these measured patterns is shown for the air-filled case.

The array was fed using a 0° four-way power splitter (Mini-Circuits ZN4PD1-183 W-S+) as seen in Figure 10. A custom-designed 3D printed mount was fabricated to hold the antenna elements in place. The measured S_{11} of the array under different channel filling conditions used in this work is plotted in Figure 11 from 3 to 10 GHz. The S_{11} response

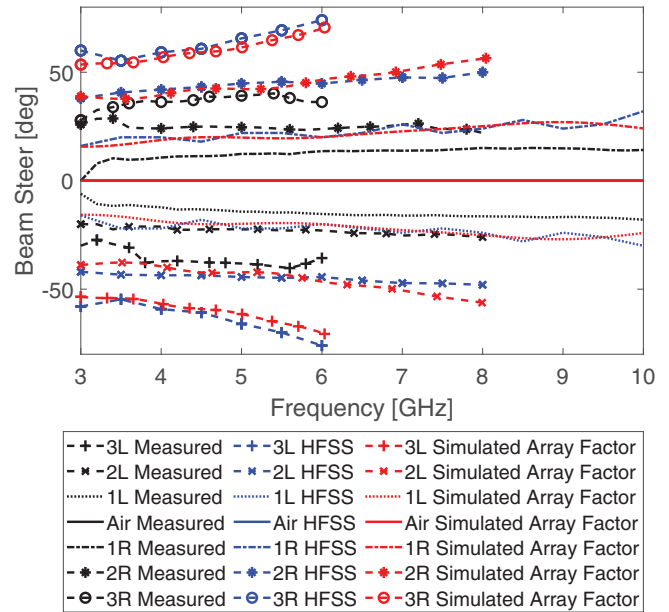


FIGURE 13 Measured (black), HFSS simulated (blue), and predicted beam steering based on the simulated phase shift data presented in Figure 3 (red) [Color figure can be viewed at wileyonlinelibrary.com]

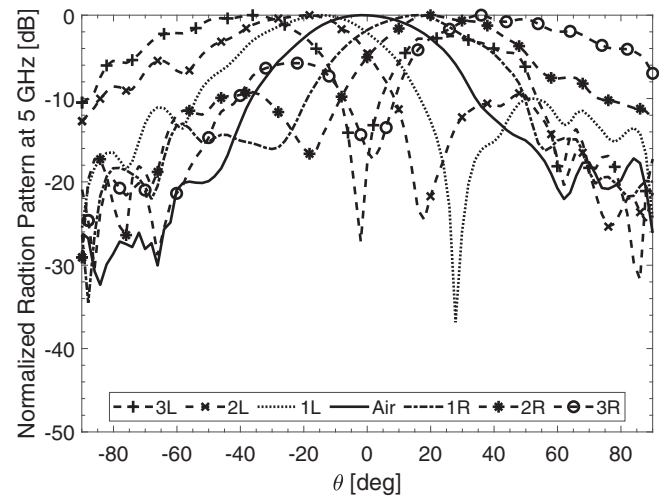


FIGURE 14 Measured radiation patterns showing normalized gain for seven levels of beam steering at 5 GHz

of the array is better than that of the single element primarily as a result of the four-way power splitter.

Radiation pattern measurements taken over the 3 to 10 GHz band and for the seven channel-filling configurations depicted in Figure 6 are summarized in Figures 12 and 13. Water is a known lossy fluid and all antenna peak gain plot in Figure 12 shows measured realized gain that has not been normalized to specifically show what the losses do to the array gain vs frequency. The air-filled array has a maximum realized gain of 13.1 dBi at 8.5 GHz and with beam steering the maximum gain decreased as more water was

added. Here the L filling cases have a larger realized gain than the R filling cases. The measured and simulated beam-steering behavior of the array over the 3 to 10 GHz band is

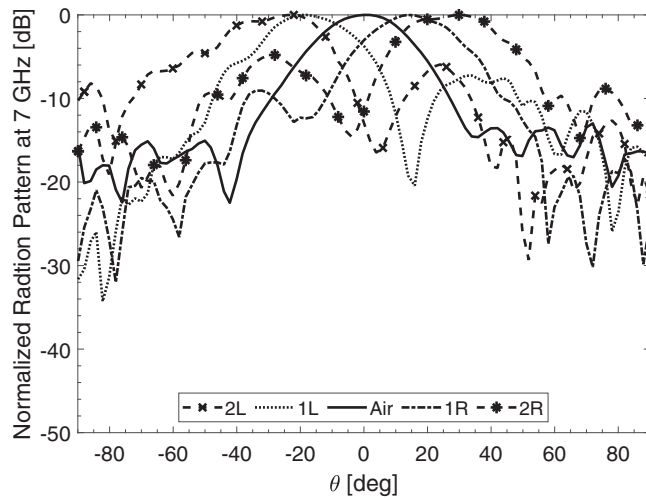


FIGURE 15 Measured radiation patterns showing normalized gain for five levels of beam steering at 7 GHz

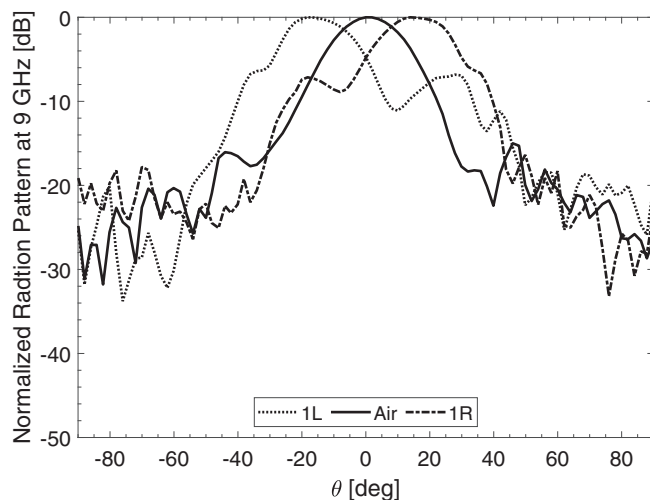


FIGURE 16 Measured radiation patterns showing normalized gain for three levels of beam steering at 9 GHz

shown in Figure 13. Below 6 GHz, the beam-steering range is about 90° between the 3R and 3L cases. At 8 GHz the useful beam-steering range drops to 50° and at 10 GHz the useful beam-steering range is 30° , where *useful* means that peak gain of the steered beam is 8 dBi or better.

From Figure 13, the L cases also have less beam steer than the respective R cases. This suggests that the volume of water between the two setups was not identical since the channels were manually filled using a syringe. Additionally, this imperfect filling helps to explain the difference between the simulated and the measured beam steering in Figure 13. This could be improved in future works by using more sophisticated water routing techniques like electrostatic routing of water droplets.⁸ This improvement in fluidic control could help to increase the beam steer to that of the simulation in Figure 13.

Representative radiation pattern measurements are shown at 5 GHz, 7 GHz, and 9 GHz under various channel-filling configurations to characterize the array's beam-steering response. At 5 GHz (Figure 14) all seven states of beam steering can be used without excessive losses due to water. This allows for seven discrete steps of beam steering for a total maximum beam steer of nearly 90° .

Further, at 7 GHz (Figure 15) water is lossier than at 5 GHz and the antenna gain is adversely impacted as the number of water-filled channels increases. The usable beam-steering range for the array at 7 GHz has a maximum of around 50° with a five discrete steps of beam steer as only two channels of phase progression can be used between elements.

Finally, at 9 GHz (Figure 16) the losses incurred due to water increase further and the usable beam-steering range is limited to only one channel of phase progression between each element, allowing for only three beam-steering states. This shows approximately 40° of beam steer across the three useful states.

Table 1 specifically compares this work to other homogeneous and isotropic fluidic beam-steering structures but independent of the antenna-element type. As shown in the table, the proposed array exhibits the largest bandwidth, highest gain and sharpest half-power beamwidth.

TABLE 1 Performance comparison with fluidic beam-steering structures

Ref.	Antenna element	Fluid used	Freq. (GHz)	Scan angle	Gain (dBi)	HPBW ^a
This study	Vivaldi	Water	3-6.5	90°	12.0	40°
			6.5-10	40°	13.1	40°
1	Patch	Water	2.55-2.65	40°	5.7	65°
3 ^b	Patch	Water	8	36°	–	–
2	Yagi-Uda	Metal ^c	1.76-1.84	360°	–	90°
4	Patch	Metal	5	45°	5.4	50°

^aHalf-power beamwidth.

^bSimulation results only.

^cMetal slugs in oil-filled channel.

4 | CONCLUSION

A four-element wideband antipodal Vivaldi Antenna array operating over 3 to 10 GHz that uses water as a high relative permittivity fluid to make a reconfigurable antenna array was designed, fabricated and measured. Water is a known lossy fluid and all antenna gain plots in this work show measured realized gain that has not been normalized to specifically emphasize what the losses do to the array gain vs frequency and beam-steering angle. The findings reveal that despite the losses of deionized (DI) water, the array can deliver a competitive gain and a beam-steering range of $\pm 45^\circ$ (90° equivalent) from 3 to 6.5 GHz and $\pm 20^\circ$ out to 10 GHz.

ACKNOWLEDGMENT

I.G. is a recipient of the Ontario Graduate Scholarship from the Province of Ontario, Canada, and the Ian M. Drum Scholarship at Queen's University. This work was supported, in part, by grant #RGPIN-2016-04784 from the Natural Sciences and Engineering Research Council of Canada (NSERC).

ORCID

Ian Goode  <https://orcid.org/0000-0001-9889-1865>

REFERENCES

- [1] Naqvi AH, Lim S. A beam-steering antenna with a fluidically programmable metasurface. *IEEE Trans Antennas Propag.* 2019;67(6):3704-3711.
- [2] Rodrigo D, Jofre L, Cetiner BA. Circular beam-steering reconfigurable antenna with liquid metal parasitics. *IEEE Trans Antennas Propag.* 2012;60(4):1796-1802.
- [3] Goode I, Saavedra C. A four element phased patch antenna array using fluidic phase shifter. *XXXIIInd General Assembly and Scientific Symposium of the International Union of Radio Science*; Montreal, Quebec, Canada: IEEE; 2017:1-2.
- [4] Bhattacharjee T, Jiang H, Behdad N. Fluidic beam steering in parasitically coupled patch antenna arrays. *Electron Lett.* 2015;51(16):1229-1231.
- [5] Brown M, Goode I, Saavedra CE. Lumped-element circuit modeling of microfluidic channels in microstrip transmission lines. *2018 16th IEEE International New Circuits and Systems Conference*; Montreal, Quebec, Canada: IEEE; 2018:31-34.
- [6] Meineri P, Dubuc D, Grenier K. Liquid-based tunable loaded-line phase shifter. *2012 9th European Radar Conference*; Amsterdam: IEEE; 2012:393-396.
- [7] Ulaby FT, Long DG, Blackwell WJ, et al. *Microwave Radar and Radiometric Remote Sensing*. Vol 4. Ann Arbor, MI: University of Michigan Press; 2014.
- [8] Cho SK, Fan SK, Moon H, Kim CJ. Towards digital microfluidic circuits: creating, transporting, cutting and merging liquid droplets by electrowetting-based actuation. *IEEE International Conference on MEMS*; Las Vegas, NV, USA: IEEE; 2002:32-35.

How to cite this article: Goode I, Saavedra CE. Ultra-wideband fluidically steered antipodal Vivaldi antenna array. *Microw Opt Technol Lett.* 2020;1-7. <https://doi.org/10.1002/mop.32398>